J Nanopart Res (2019) 21: 48
https://doi.org/10.1007/s11051-019-4493-6

TECHNOLOGY AND APPLICATION

Preparation and catalytic activities of $CuFe_2O_4$ nanoparticles assembled with graphene oxide for RDX thermal decomposition

Bo Liu · Weimin Wang · Jingjing Wang · Yu Zhang · Kangzhen Xu · Fengqi Zhao

Received: 17 December 2018 / Accepted: 19 February 2019 / Published online: 2 March 2019

Abstract A graphene oxide-based nano-metal composite oxide $CuFe_2O_4$/GO was successfully prepared by a versatile self-assembly approach. Structure and morphological characterization of $CuFe_2O_4$/GO nanocomposite were studied in detail by a series of characterization techniques including XRD, FT-IR, XPS, BET, SEM, and TEM. The results revealed that the self-assembly process did not destroy the composition and morphology of the spinel-structured $CuFe_2O_4$ particle, and the transparent GO sheets with wrinkled and rough texture are tightly coated on the surface of $CuFe_2O_4$ nanoparticles like a layer of thin gauze clothing. The particle size of $CuFe_2O_4$ is about 200 nm. Catalytic activity of as-prepared $CuFe_2O_4$/GO nanocomposite on the thermal decomposition of cyclotrimethylene trinitramine (RDX) was investigated via differential scanning calorimetry (DSC). The experimental results show that the $CuFe_2O_4$/GO nanocomposite has much higher catalytic activity than single $CuFe_2O_4$ nanoparticles and GO. Thermal decomposition temperature and apparent activation energy of RDX were reduced from 241.27 to 220.34 °C and from 172.6 to 142.56 kJ mol^{-1}, respectively. The improved performance could be attributed to the "positive synergistic effect" between $CuFe_2O_4$ nanoparticles and GO.

B. Liu · W. Wang · J. Wang · Y. Zhang · K. Xu (✉)
School of Chemical Engineering, Northwest University, Xi'an 710069, China
e-mail: xukz@nwu.edu.cn

F. Zhao
Xi'an Modern Chemistry Research Institute, Xi'an 710065, China

Keywords Nanomaterials · Graphene oxide · Metal composite oxide · Self-assembly · Catalytic decomposition · Nanostructured catalysts

Introduction

Solid composite propellants are usually composed of binders, energetic fuel additives, oxidizers, and combustion catalysts. Its combustion is a complex transfer process of mass and energy (Kapoor et al. 2009; Singh et al. 2000; Lan et al. 2015). Cyclotrimethylene trinitramine (RDX) is a common oxidizer in solid composite propellants, and its thermal decomposition performance greatly influences the burning behavior of propellants: reducing the thermal decomposition temperature and the apparent activation energy, shortening the ignition delay time and increasing the combustion rate (Bu et al. 2018; Ebrahim et al. 2012; Zhang et al. 2015). It is a fact that the lower the decomposition temperature is, the higher the burning rate is (Li et al. 2013; Fitzgerald and Brewster 2004). The performance of solid composite propellants can be significantly improved by adding a small quantity of combustion catalysts in propellants, especially nano-sized catalysts due to their smaller size, larger specific surface area, and higher catalytic activity, including nano-sized metals, nano-sized metal oxides, and their composites (Armstrong et al. 2003; Yuan et al. 2014; Ilhan et al. 2015).

Spinel ferrites are fascinating materials in the world of nano-regime with a general formula MFe_2O_4, where M represents a class of divalent metal cations such as

Cu, Mg, and Co. Copper ferrite ($CuFe_2O_4$) is a kind of spinel ferrite materials with tetragonal structure or cubic structure depending on the preparation conditions (Rashad et al. 2012; Sultan and Singh 2009; Phuruangrat et al. 2016). In certain technological conditions, the tetragonal structure of $CuFe_2O_4$ could be converted into cubic phase, such as at temperature below 300 °C (Nedkov et al. 2006) or rapid cooling from high temperature (above 760 °C) (Kim et al. 2004). Cation distribution affects the properties of the spinel ferrite materials to some extent. The copper ferrite ($CuFe_2O_4$) as a magnetic p-type semiconductor with narrow band gap has attracted great attention because of its excellent magnetic properties, high electric conductivity, and high thermal stability and catalytic activity. It has been widely investigated and used in electrode materials (Yeh and Shen 2008), high density magnetic optic recording devices (Kim et al. 2004; Kurian and Mathew 2017), magnetic resonance imaging (Kurian and Mathew 2017), drug-loading materials (Arias et al. 2008), and catalytic uses (Rashad et al. 2012). In this work, the copper ferrite ($CuFe_2O_4$) with the cubic spinel structure was successfully prepared by a one-step solvothermal method.

Nanoparticles with high density of surface-active sites and excellent catalytic performance usually tend to agglomerate and thus reducing its catalytic activity. The self-assembled method is widely used in the preparation of carbon-based nanocomposite materials due to its simple and efficient properties (Tao et al. 2017; Thiruvengadathan et al. 2014; Zhang et al. 2016a, b). Graphene oxide (GO) is a derivative of graphene and was frequently used as substrate for composite materials with better performance in recent years (Zhu et al. 2010a, b). In this work, $CuFe_2O_4$/GO nanocomposite combustion catalyst was fabricated by a versatile self-assembly method. GO in the nanocomposite can not only inhibit the agglomeration of nanoparticles, but also accelerate the charge transportation and enhance the catalytic performance of the nanocomposite owing to its excellent properties (Chen et al. 2016; Li et al. 2012).

Experimental section

Reagents and materials

All the AR-chemical reagents were commercially available and used as received without further purification. Graphene oxide (GO) was prepared from natural graphite basing on a modified Hummer's method (Marcano et al. 2010; Li et al. 2018). RDX was provided by the Xi'an Modern Chemistry Research Institute.

Materials synthesis

The $CuFe_2O_4$ nanoparticles were synthesized according to a one-pot solvothermal method previously reported by our group (Zhang et al. 2015). Briefly, 4 mmol of $CuCl_2{\cdot}2H_2O$, 8 mmol of $FeCl_3{\cdot}6H_2O$, 12 mmol of NaAc, and 1.0 g of PVP (the molar ratio of Cu:Fe is 1:2) were dissolved in 70 ml of ethylene glycol and stirred vigorously for 1 h. The mixture solution was sealed in a 100 mL Teflon-lined stainless steel autoclave, held at 180 °C for 12 h and allowed to cool to room temperature. Finally, the as-obtained black precipitate was centrifuged, washed with ethanol and deionized water several times, and dried at 60 °C in a vacuum oven for 24 h.

The $CuFe_2O_4$/GO nanocomposite was prepared by a versatile self-assembly approach (Thiruvengadathan et al. 2014). The detailed preparation processes were as follows: 30 mg of GO powder was dispersed in 30 mL deionized water and sonicated for 2 h to form a brown GO aqueous solution with a concentration of about 1 mg mL^{-1} for later use. 0.3 g of as-prepared $CuFe_2O_4$ nanoparticles was dispersed in deionized water with sonication for 1 h to be a homogeneously dispersed suspension, and the pH value of this suspension was adjusted to four using 0.1 mol L^{-1} HCl solution. Subsequently, the resulting GO aqueous solution was then added to the above suspension dropwise and the mixed solution was sonicated for another 2 h. Finally, the obtained $CuFe_2O_4$/GO nanocomposite was centrifuged, washed, and dried.

Materials characterization

The crystal structure, phase composition, and morphological and structural characterization of samples were determined by XRD, XPS, BET, SEM, and TEM. The powder X-ray diffraction (XRD) patterns in the 2θ range of 5°–80° were recorded on a Rigaku Mini Flex 600 X-ray diffractometer using Cu Kα radiation (λ = 0.1541 nm). X-ray photoelectron spectroscopy (XPS) measurements were carried out with a Thermo Scientific ESCALAB 250 Xi X-ray photoelectron spectrometer. The Brunauer-Emmett-Teller (BET) specific surface

area and pore volume of as-prepared samples were performed by an Autosorb-iQ automated gas sorption system. Scanning electron microscope (SEM) images were carried out using a Carl Zeiss SIGMA field emission scanning electron microscopy (FESEM). Transmission electron microscopy (TEM) and high-resolution transmission electron microscopy (HRTEM) images were measured on a FEI Tecnai G2 microscope operated at 200 kV.

Catalytic activity measurements

RDX was selected as target materials for investigating catalytic activities of the as-prepared samples. The as-prepared samples and RDX were fully mixed in the mass ratio of 1 : 4 by rubbing method. Thermal decomposition analysis of the resulting mixture was performed using a 200F3 differential scanning calorimeter (DSC) (Netzsch, Germany) at a heating rate of 10 °C min^{-1} in an N_2 atmosphere at a flow rate of 40 mL min^{-1} under ambient atmosphere pressure.

Results and discussion

Materials characterization

The powder XRD diffraction patterns of the resulting GO, $CuFe_2O_4$, and $CuFe_2O_4$/GO nanocomposite are shown in Fig. 1. The characteristic diffraction peak of GO centered at $2\theta = 12.5°$ can be assigned to the (001) reflection. The reflection peaks of as-prepared $CuFe_2O_4$ nanoparticles correspond well with the standard pattern of spinel phase of $CuFe_2O_4$ (JCPDS No. 77-0010), indicating the formation of pure spinel phase $CuFe_2O_4$. All characteristic diffraction peaks of $CuFe_2O_4$/GO nanocomposite are consistent with the pure $CuFe_2O_4$ nanoparticles. The characteristic diffraction peak of GO is not detected in the $CuFe_2O_4$/GO nanocomposite, which may be because the amount of GO is too small to detect by XRD (Noor-ul et al. 2016). The presence of GO in the nanocomposite is further demonstrated by SEM, TEM, and FT-IR that followed.

FT-IR spectra of the pure GO, the $CuFe_2O_4$ nanoparticles, and the $CuFe_2O_4$/GO nanocomposite are shown in Fig. 2. In the FT-IR spectrum of the pure GO, the characteristic peaks of oxygen-containing functional groups C=O, C-OH, and C-O-C are at 1725 cm^{-1}, 1398 cm^{-1}, and 1058 cm^{-1}, respectively (Zhu et al. 2010a, b). The

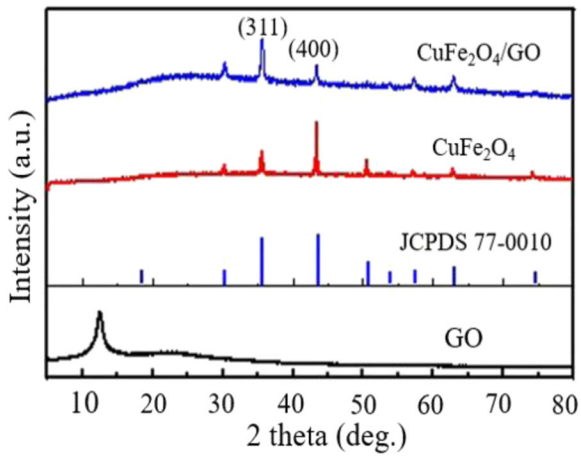

Fig. 1 Powder XRD patterns of GO, $CuFe_2O_4$, and $CuFe_2O_4$/GO nanocomposite

peak appeared at 1623 cm^{-1} is attributed to the skeletal vibration of aromatic domains (Meidanchi and Akhavan 2014). The broad peak located at 3422 cm^{-1} is assigned to the stretching vibration mode of O-H in adsorbed water molecules and the oxygen-containing functional groups on the surface of GO sheets. In the $CuFe_2O_4$ nanoparticles, the peak observed at about 438 cm^{-1} can be attributed to octahedral Cu^{2+} (Cu-O mode) stretching vibration, and the peak at about 620 cm^{-1} can be assigned to tetrahedral Fe^{3+} (Fe-O mode) stretching vibration (Phuruangrat et al. 2016). In the $CuFe_2O_4$/GO nanocomposite, it can be clearly observed that there exist the characteristic peaks of GO and $CuFe_2O_4$ nanoparticles. The results of both XRD and FT-IR indicate that the $CuFe_2O_4$/GO nanocomposite was successfully prepared via a versatile self-assembly approach.

The morphology and the structure of the $CuFe_2O_4$ nanoparticles and the assembled $CuFe_2O_4$/GO nanocomposite were characterized by SEM (Fig. 3). From Fig. 3(a), it can be seen that the as-prepared $CuFe_2O_4$ nanoparticles have a well-defined spherical structure and a small size distribution with an average particle size of 200 nm, and exhibit rough surfaces, which is beneficial to enhancing the interaction between GO sheets and $CuFe_2O_4$ nanoparticles. In the $CuFe_2O_4$/GO nanocomposite, it can be clearly seen that the GO sheets are tightly wrapped on the surfaces of $CuFe_2O_4$ nanoparticles like a layer of thin gauze clothing, forming a three-dimensional (3D) interconnected network structure between particles. The self-assembly process did not destroy the composition and morphology of the spinel-structured $CuFe_2O_4$ particles. The most important point is that GO sheets and

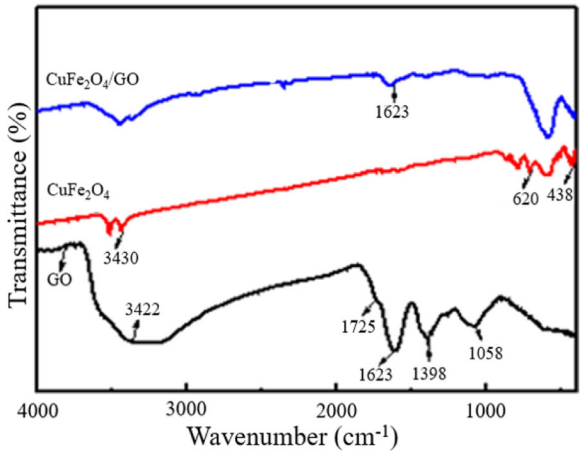

Fig. 2 FT-IR spectra of GO, $CuFe_2O_4$, and $CuFe_2O_4$/GO nanocomposite

$CuFe_2O_4$ nanoparticles touch each other a lot, and little separation could be observed in the $CuFe_2O_4$/GO nanocomposite. This is beneficial to preventing $CuFe_2O_4$ nanoparticles from agglomeration and increasing the surface-active sites of $CuFe_2O_4$ nanoparticles, thereby improving the catalytic performance of the nanocomposite. The Brunauer-Emmett-Teller (BET) specific surface area and pore volume of the samples are shown in Table 1. The BET surface area and the total pore volume of $CuFe_2O_4$/GO nanocomposite are found to be 45.27 $m^2\ g^{-1}$ and 0.106 $cm^3\ g^{-1}$, respectively, which are higher than those of $CuFe_2O_4$. This is consistent with the analysis of SEM.

The crystal structure of the $CuFe_2O_4$/GO nanocomposite and visualized effects of self-assembly were further investigated by TEM (Fig. 4). The same morphology and structure could be observed as SEM images. The TEM images [Fig. 4(a, b)] showed that the $CuFe_2O_4$ particles with an average size around 200 nm consist of lots of smaller primary nanocrystals. The middle of the $CuFe_2O_4$ particle is lighter relative to its edge, implying its hollow nano-spherical structure feature. The $CuFe_2O_4$ particles are wrapped tightly by transparent GO sheets, forming a three-dimensional (3D) network structures. It is clear that the transparent GO sheets with lots of wrinkles exist on the edge of $CuFe_2O_4$/GO nanocomposite. The unique structure feature of the $CuFe_2O_4$/GO nanocomposite could effectively prevent from combining of electrons and holes in the catalytic decomposition process of RDX, which provides an excellent pathway of charge transfer and accelerate the transfer of electrons, so the structure feature of $CuFe_2O_4$/GO nanocomposite is beneficial to accelerating the catalysis process and enhancing its catalytic performance (Li et al. 2013; Zu et al. 2016). In the HRTEM images [Fig. 4(c, d)], the interplanar spacings of 0.251 and 0.210 nm correspond to the lattice fringe spacings of the (311) and (400) diffraction planes for the spinel $CuFe_2O_4$ (JCPDS No. 77-0010), respectively, which suggests that $CuFe_2O_4$ particles in the $CuFe_2O_4$/GO nanocomposite have a well-defined crystallinity. The TEM and HRTEM results further confirm that the $CuFe_2O_4$/GO nanocomposite was prepared by a versatile self-assembly approach.

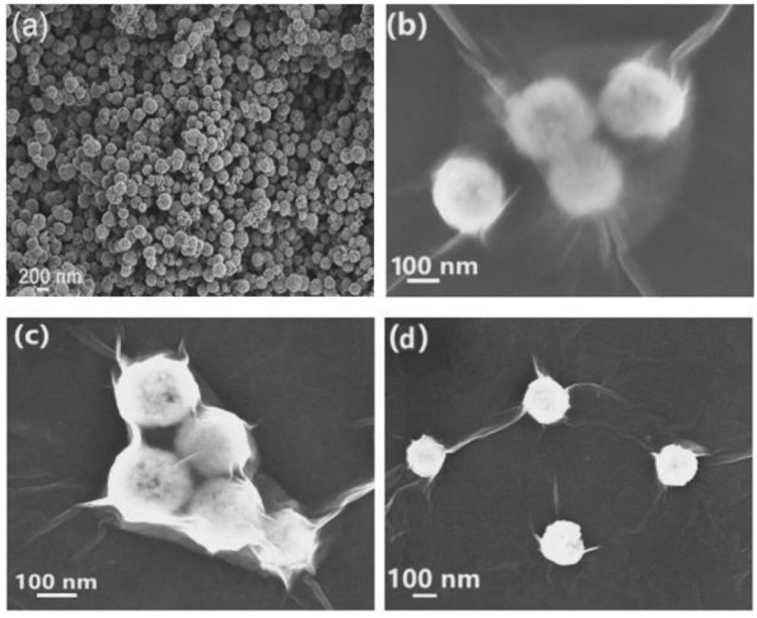

Fig. 3 SEM images of $CuFe_2O_4$/GO nanocomposite

Table 1 Textural properties of $CuFe_2O_4$ and $CuFe_2O_4$/GO nanocomposite

Sample	S_{BET}[a] ($m^2\ g^{-1}$)	V_{total}[b] ($cm^3\ g^{-1}$)	D_{aver} (nm)
$CuFe_2O_4$	32.66	0.093	11.36
$CuFe_2O_4$/GO	45.27	0.106	10.74

[a] The specific surface area calculated by the BET method

[b] Total pore volume calculated at $p/p_0 = 0.95$

To reveal the surface elementary composition and the chemical states of elements of the $CuFe_2O_4$/GO nanocomposite, X-ray photoelectron spectroscopy (XPS) measurement was taken. The survey spectrum, the copper (Cu 2p), iron (Fe 2p), oxygen (O 1 s), and carbon (C 1 s) spectra were analyzed (Fig. 5). In the survey spectrum, it can be seen that there are four elements Cu, Fe, O, and C in the $CuFe_2O_4$/GO nanocomposite [Fig. 5(a)]. In Fig. 5(b), the two binding energy peaks at 933.2 eV for Cu $2p_{3/2}$ and 953.5 eV for Cu $2p_{1/2}$ with a shake-up satellite peak at about 950 eV indicate the presence of the Cu(II) oxidation state in the composite (Nedkov et al. 2006; Tang et al. 2016). For Fe 2p spectrum [Fig. 5(c)], two prominent peaks with binding energy value of 710.9 ev and 724.6 eV can be assigned to the spectra of Fe 2p3/2 and Fe 2p1/2, respectively, indicating the Fe (III) oxidation state of $CuFe_2O_4$ in the $CuFe_2O_4$/GO nanocomposite (Zu et al. 2016; Shu et al. 2018). The high-resolution O 1s spectrum in the nanocomposite can be divided into three main peaks [Fig. 5(d)]. The peak centered at 530.6 eV is assigned to the lattice oxygen in the crystal lattice of $CuFe_2O_4$ particle (Zhou et al. 2015). The peaks located at 532.3 eV and 533.6 eV are attributed to the C-O and C-O-C, respectively, in GO (Krishnamoorthy et al. 2013; Ding et al. 2018). The high-resolution C 1s spectrum of $CuFe_2O_4$/GO nanocomposite shown in Fig. 5(e) consists of three main components: C-C/C=C (284.8 eV) in the aromatic rings, C-O (286.6 eV) of epoxy and alkoxy, and C=O (289.3 eV) groups (Zhang et al. 2016a, b). The above results further confirm that GO and $CuFe_2O_4$ nanoparticles were successfully assembled together, and the $CuFe_2O_4$/GO nanocomposite formed.

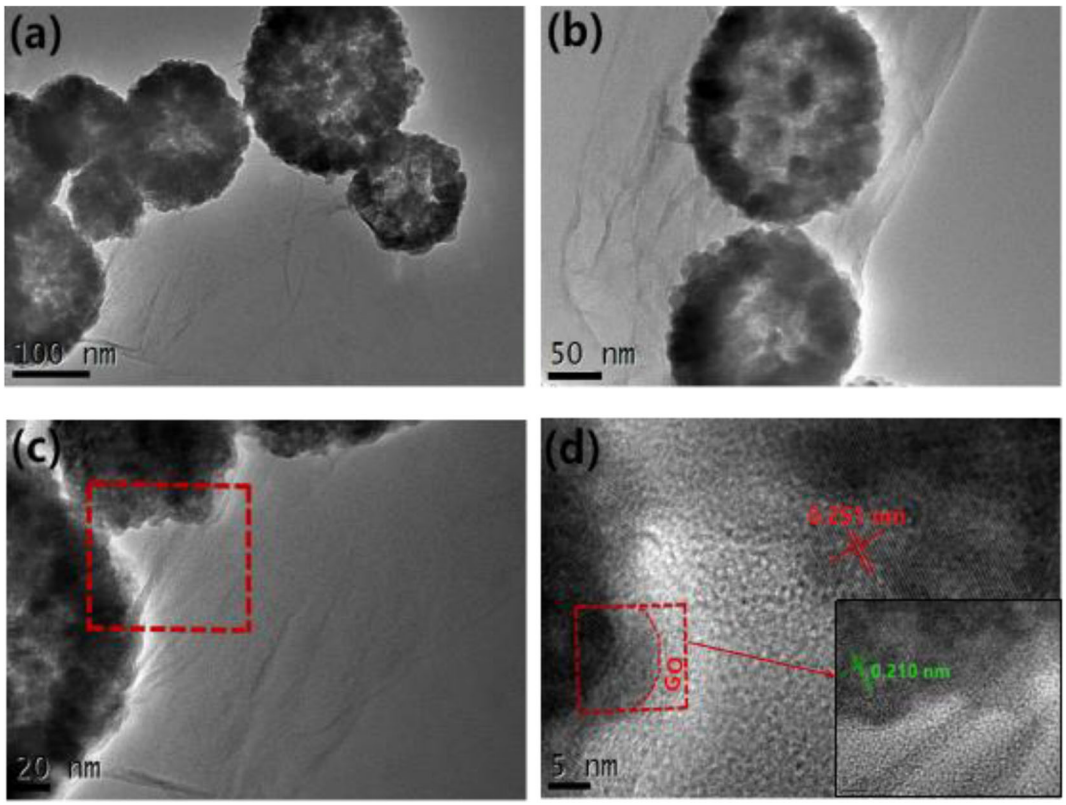

Fig. 4 TEM and HRTEM images of $CuFe_2O_4$/GO nanocomposite

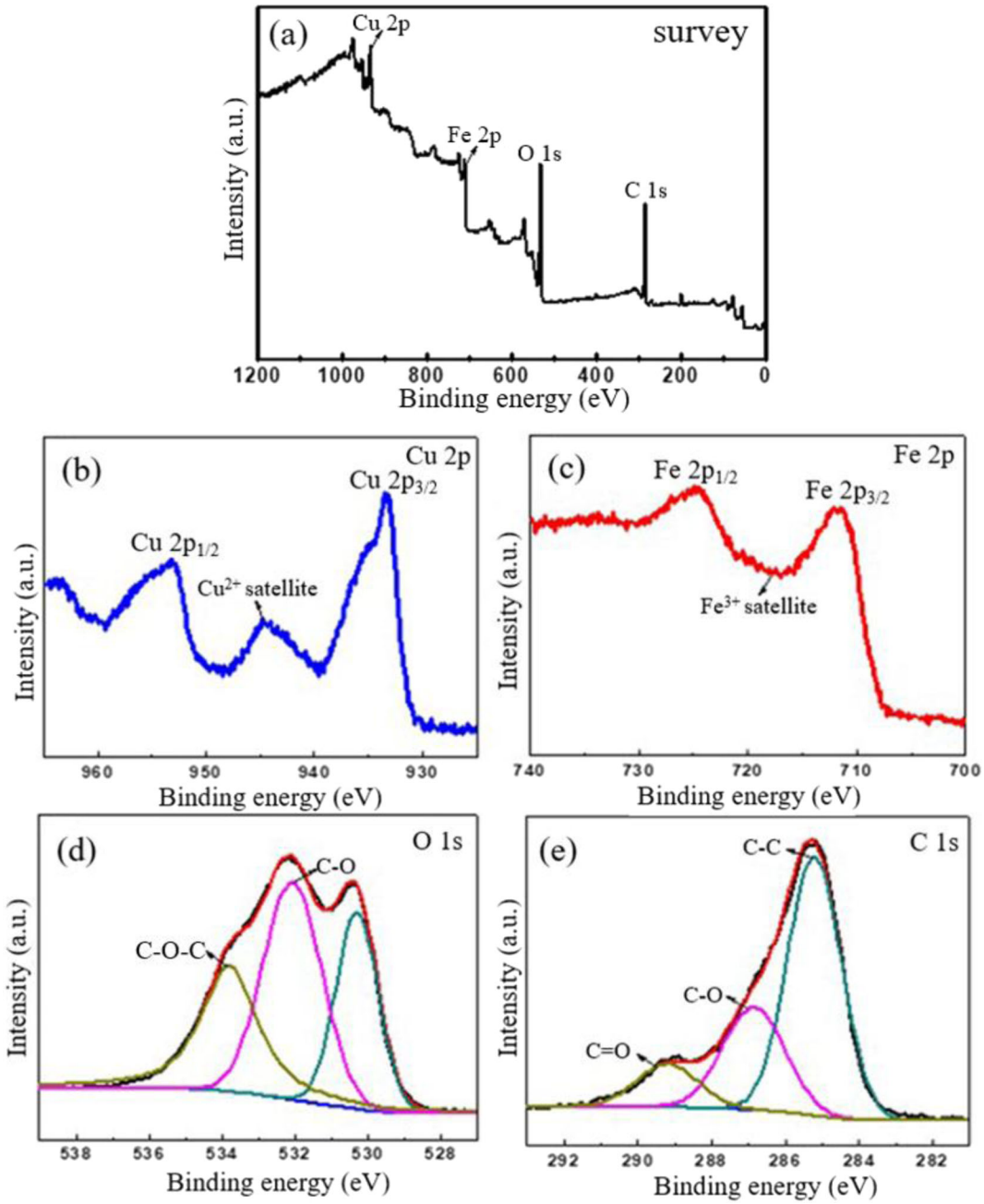

Fig. 5 X-ray Photoelectron spectroscopy of $CuFe_2O_4$/GO nanocomposite: (a) survey spectra, (b) Cu 2p, (c) Fe 2p, (d) O 1 s, and (e) C 1 s

The influence on the thermal decomposition of RDX

Cyclotrimethylene trinitramine (RDX) as a frequently used high-energy explosive is one of the major ingredients in composite solid propellants (Zhang et al.2015), and its thermal decomposition properties directly influence the combustion behavior of the propellants. In order to further investigate the catalytic decomposition performance of the $CuFe_2O_4$/GO nanocomposite catalyst for RDX, the as-prepared nanomaterials were explored as a potential burning additive of the thermal decomposition of RDX. The catalytic performance of GO, pure $CuFe_2O_4$, and self-assembled $CuFe_2O_4$/GO nanocomposite was investigated by DSC analysis at a

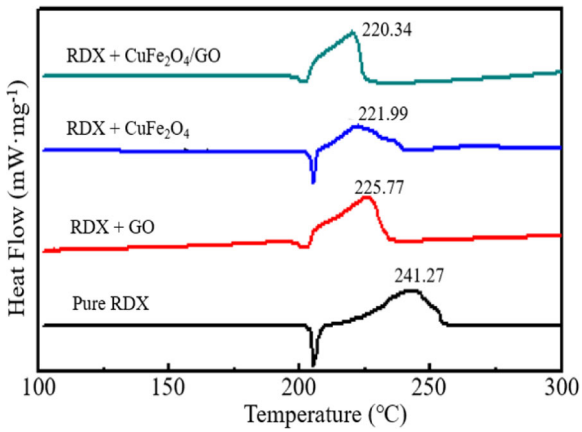

Fig. 6 DSC curves of pure RDX and RDX mixed with GO, $CuFe_2O_4$, and $CuFe_2O_4$/GO

heating rate of 10 °C min^{-1} from room temperature to 300 °C in an N_2 atmosphere at a flow rate of 40 ml min^{-1} under ambient atmosphere pressure. The apparent activation energy of the catalytic decomposition process was calculated by Kissinger method and Ozawa method with DSC data at different heating rates (5.0, 10.0, 15.0, and 20.0 °C min^{-1}) (Kissinger 1957; Ozawa 1965). The samples for DSC analysis were prepared as follows: the as-synthesized GO, $CuFe_2O_4$, and $CuFe_2O_4$/GO nanocomposite were fully mixed with RDX in the mass ratio of 1 : 4, respectively, and ground gently in an agate mortar to the good uniformity; sample mass, approximately 0.5 mg.

The DSC curves of pure RDX and the mixtures of as-obtained powders with RDX are shown in Fig. 6. The exothermic peak temperatures of the decomposition processes are used to evaluate the catalytic effect of pure GO, $CuFe_2O_4$, and self-assembled $CuFe_2O_4$/GO nanocomposite on RDX. The peak temperatures of RDX, RDX+GO, RDX+$CuFe_2O_4$, and RDX+$CuFe_2O_4$/GO nanocomposite are 241.27, 225.77, 221.99, and 220.34 °C, respectively. Compared with the pure RDX, the peak temperatures of RDX+GO, RDX+$CuFe_2O_4$, and RDX+$CuFe_2O_4$/GO nanocomposite reduce by 15.50, 19.28, and 20.93 °C, respectively, indicating that pure GO, $CuFe_2O_4$, and self-assembled $CuFe_2O_4$/GO nanocomposite have catalytic effect on the thermal decomposition of RDX, and the $CuFe_2O_4$/GO nanocomposite has the best catalytic effect among them. An exothermic peak located at 205 °C is attributed to the melting of RDX, with no significant change in all DSC curves. In addition, the apparent activation energy of the catalytic thermal decomposition for $CuFe_2O_4$/GO nanocomposite calculated by Kissinger method and Ozawa method is 142.56 and 143.32 kJ mol^{-1}, respectively, which is approximately equal. Compared with the value of pure RDX (172.6 kJ mol^{-1}) reported in the previous literature (Zhang et al. 2015), it is significantly reduced by about 30 kJ mol^{-1}. The above results indicate that the as-prepared self-assembled $CuFe_2O_4$/GO nanocomposite has excellent catalytic performance, which can be attributed to the excellent conductivity of GO in the $CuFe_2O_4$/GO nanocomposite and the "positive synergistic effect" between GO sheets and $CuFe_2O_4$ nanoparticles in the $CuFe_2O_4$/GO nanocomposite.

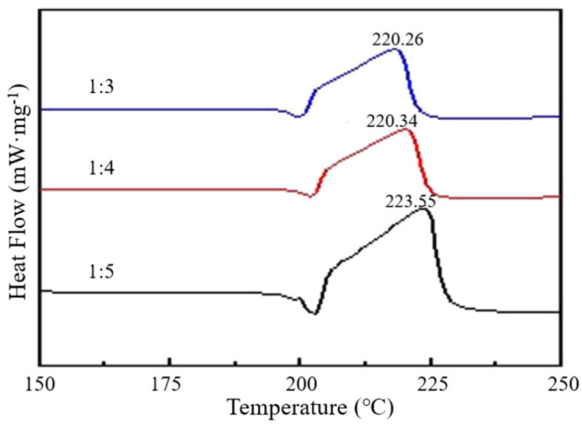

Fig. 7 DSC curves of RDX mixed with $CuFe_2O_4$/GO in different mass ratios

Figure 7 shows the DSC curves of RDX mixed with $CuFe_2O_4$/GO nanocomposite in different mass ratios at a heating rate of 10 °C. The exothermic peak temperatures of catalytic thermal decomposition for $CuFe_2O_4$/GO + RDX (1:3), $CuFe_2O_4$/GO + RDX (1:4), and $CuFe_2O_4$/GO + RDX (1:5) are 220.26, 220.34, and 223.55 °C, respectively, all decreasing by 21.01, 20.93, and 17.72 °C compared with the pure RDX (241.27 °C). Among them, the decomposition peak temperatures of the $CuFe_2O_4$/GO + RDX (1:3) and $CuFe_2O_4$/GO + RDX (1:4) systems are almost equal. Therefore, we use RDX + $CuFe_2O_4$/GO (1:4) as the best mixing ratio in this work.

Conclusion

In summary, we successfully prepared $CuFe_2O_4$/GO nanocomposite by a versatile self-assembly approach and studied its catalytic decomposition performance for RDX. $CuFe_2O_4$ nanoparticles modified by H^+ ions were tightly

coated by GO sheets, which could effectively prevent $CuFe_2O_4$ nanoparticles from aggregating. The self-assembly process did not destroy the composition and morphology of the spinel-structured $CuFe_2O_4$ particles. The excellent conductivity of GO in the $CuFe_2O_4$/GO nanocomposite could also accelerate the transfer of electrons during the catalytic thermal decomposition process of RDX, which further enhances its catalytic performance. The DSC results show that the self-assembled $CuFe_2O_4$/GO nanocomposite can significantly reduce the exothermic peak temperature and the apparent activation energy of RDX from 241.27 to 220.34 °C and from 172.6 to 142.56 kJ mol^{-1}, respectively. The $CuFe_2O_4$/GO nanocomposite exhibits excellent catalytic decomposition activity and good application performance in composite solid propellant, and the catalytic effect of $CuFe_2O_4$/GO nanocomposite on the thermal decomposition of RDX is higher than those of single-$CuFe_2O_4$ nanoparticles and GO sheets. In addition, this effective, scalable, and environmentally benign route for preparing $CuFe_2O_4$/GO nanocomposite can also be expanded to prepare other GO-based functional nanomaterials used as catalysts, superior anode materials for lithium-ion batteries, and other fields.

Funding information This investigation received financial assistance from the National Defense Key Laboratory of China and the Natural Science Foundation of Shaanxi Province (2018JM5181).

Compliance with ethical standards

Conflict of interest The authors declare that they have no conflict of interest.

References

Arias JL, Ruiz MA, Gallardo V, Delgado AV (2008) Tegafur loading and release properties of magnetite/poly(alkylcyanoacrylate) (core/shell) nanoparticels. J Control Release 125:50–58

Armstrong RW, Baschung B, Booth DW, Samirant M (2003) Enhanced propellant combustion with nanoparticles. Nano Lett 3:253–255

Bu XH, Liu FY, Zhang ZW, Wang ZZ, Liu JH, Liu W (2018) Facile synthesis of flower-like ZnO@Fe_2O_3 hierarchical nanostructures with enhanced catalytic activity on the thermal decomposition of ammonium perchlorate. Mater Lett 219:33–36

Chen P, Xing X, Xie HF, Sheng Q, Qu HX (2016) High catalytic activity of magnetic $CuFe_2O_4$/graphene oxide composite for the degradation of organic dyes under visible light irradiation. Chem Phys Lett 660:176–181

Ding GH, Zhang NN, Wang CC, Li XY, Zhang J, Li WR, Li RJ, Yang ZN (2018) Effect of the size on the aggregation and sedimentation of graphene oxide in seawaters with different salinities. J Nanopart Res 20:313–322

Ebrahim AG, Shaabani B, Khodayari A, Yashar AK, Rahimi R (2012) Investigation of the catalytic activity of nano-sized CuO, Co_3O_4 and $CuCo_2O_4$ powders on thermal decomposition of ammonium perchlorate. Powder Technol 217:330–339

Fitzgerald RP, Brewster MQ (2004) Flame and surface structure of laminate propellants with coarse and fine ammonium perchlorate. Combust Flame 3:313–326

IIhan S, Izotova SG, Komlev AA (2015) Synthesis and characterization of $MgFe_2O_4$ nanoparticles prepared by hydrothermal decomposition of co-precipitated magnesium and iron hydroxides. Ceram Int 41:577–585

Kapoor IPS, Srivastava P, Singh G (2009) Nanocrystalline transition metal oxides as catalysts in the thermal decomposition of ammonium perchlorate. Propellants Explos Pyrotech 34:351–356

Kim KJ, Lee JH, Lee SH (2004) Magneto-optical investigation of spinel ferrite $CuFe_2O_4$: observation of Jahn-Teller effect in Cu^{2+} ion. J Magn Magn Mater 279:173–177

Kissinger HE (1957) Reaction kinetics in differential thermal analysis. Anal Chem 29:1702–1706

Krishnamoorthy K, Veerapandian M, Yun K, Kim SJ (2013) The chemical and structure analysis of graphene oxide with different degrees of oxidation. Carbon 53:38–49

Kurian J, Mathew MJ (2017) A facile approach to the elucidation of magnetic parameters of $CuFe_2O_4$ nanoparticles synthesized by hydrothermal route. J Magn Magn Mater 428:204–212

Lan YF, Li XY, Li GP, Luo YJ (2015) Sol-gel method to prepare graphene/Fe_2O_3 aerogel and its catalytic application for the thermal decomposition of ammonium perchlorate. J Nanopart Res 17:395–403

Li BX, Liu TX, Wang YF, Wang ZF (2012) ZnO/graphene-oxide nanocomposite with remarkably enhanced visible-light-driven photocatalytic performance. J Colloid Interface Sci 377:114–121

Li N, Geng ZF, Cao MH, Ren L, Zhao XY, Liu B, Tian Y, Hu CW (2013) Well-dispersed ultrafine Mn_3O_4 nanoparticles on graphene as a promising catalyst for the thermal decomposition of ammonium perchlorate. Carbon 54:124–132

Li HY, Sun C, Zhao Y, Xu XJ, HW Y (2018) Facile synthesis of recyclable Co3O4/Co(OH)2/RGO ternary heterostructures with synergistic effect for photocatalysis. J Nanopart Res 20:279–291

Marcano DC, Kosynkin DV, Berlin JM, Sinitskii A, Sun ZZ, Slesarev A, Alemany LB, Lu W, Tour JM (2010) Improved synthesis of graphene oxide. ACS Nano 4:4806–4814

Meidanchi A, Akhavan O (2014) Superparamagnetic zinc ferrite spinel-graphene nanostructures for fast wastewarter purification. Carbon 69:230–238

Nedkov I, Vandenberghe RE, Marinova T, Thailhades P, Merodiiska T, Avramova I (2006) Magnetic structure and

collective Jahn-Teller distortions in nanostructured particles of $CuFe_2O_4$. Appl Surf Sci 253:2589–2596

Noor-ul A, Shaheen W, Bashir B, Abdelsalam NM, Warsi MF, Khan MA, Shahid M (2016) Electrical, magnetic and photoelectrochemical activity of rGO/$MgFe_2O_4$ nanocomposites under visible light irradiation. Ceram Int 42:12401–12408

Ozawa T (1965) A new method of analyzing thermo-gravimetric data. Bull Chem Soc Jpn 38:1881–1885

Phuruangrat A, Kuntalue B, Thongtem S, Thongtem T (2016) Synthesis of cubic $CuFe_2O_4$ nanoparticles by microwave-hydrothermal method and their magnetic properties. Mater Lett 167:65–68

Rashad MM, Mohamed RM, Ibrahim MA, Ismail LFM, Abdel-Aal EA (2012) Magnetic and catalytic properties of cubic copper ferrite nanopowders synthesized from secondary resources. Adv Powder Technol 23:315–323

Shu RW, Zhang GY, Wang X, Gao X, Wang M, Gan Y, Shi JJ, He J (2018) Fabrication of 3D net-like MWCNTs/$ZnFe_2O_4$ hybrid composites as high-performance electromagnetic wave absorbers. Chem Eng J 337:242–255

Singh G, Kapoor IPS, Mannan SM, Kaur J (2000) Studies on energetic compounds Part 8: thermolysis of salts of HNO_3 and $HClO_4$. J Hazard Mater A79:1–18

Sultan M, Singh R (2009) Magnetization and crystal structure of RF-sputtered nanocrystalline $CuFe_2O_4$ thin films. Mater Lett 63:1764–1766

Tang MY, Xia FL, Gao CJ, Qiu HX (2016) Preparation of magnetically recyclable $CuFe_2O_4$/RGO for catalytic hydrolysis of sodium borohydride. Int J Hydrog Energy 41:13058–13068

Tao Y, Zhang JL, Yang YY, Wu HX, Hu L, Dong XH, Lu J, Guo SW (2017) Metastable intermolecular composites of Al and CuO nanoparticles assembled with graphene quantum dots. RSC Adv 7:1718–1723

Thiruvengadathan R, Chung SW, Basuray S, Balasubramanian B, Staley CS, Gangopadhyay K, Gangopadhyay S (2014) A versatile self-assembly approach toward high performance nanoenergetic composite using functionalized graphene. Langmuir 30:6556–6564

Yeh CL, Shen YG (2008) Effects of TiC addition on formation of Ti_3SiC_2 by self-propagating high-temperatures synthesis. J Alloys Compd 458:286–291

Yuan Y, Wei J, Wang YJ, Shen P, Li FS, Li PY, Zhao FQ, Gao HX (2014) Hydrothermal preparation of Fe_2O_3/graphene nanocomposite and its enhanced catalytic activity on the thermal decomposition of ammonium perchlorate. Appl Surf Sci 303:354–359

Zhang Y, Wei TT, Xu KZ, Ren ZY, Xiao LB, Song JR, Zhao FQ (2015) Catalytic decomposition action of hollow $CuFe_2O_4$ nanospheres on RDX and FOX-7. RSC Adv 5:75630–75635

Zhang N, Huang Y, Zong M, Ding X, Li SP, Wang MY (2016a) Synthesis of core-shell $ZnFe_2O_4$@SiO2 hollow microspheres/reduced graphene oxides for high-performance EM wave absorber. Ceram Int 42:18879–18886

Zhang TF, Ma Z, Li GP, Wang Z, Zhao BB, Luo YJ (2016b) Electrostatic interactions for directed assembly of high performance nanostructured energetic materials of Al/Fe_2O_3/multi-walled carbon nanotube (MWCNT). J Solid State Chem 237:394–403

Zhou X, Li XW, Sun HB, Sun P, Liang XS, Liu FM, Hu XL, Lu GY (2015) Nanosheet-assembled $ZnFe_2O_4$ hollow microspheres for high-sensitive acetone sensor. ACS Appl Mater Interfaces 7:15414–15421

Zhu YW, Murali S, Cai WW, Li XS, Suk JW, Potts JR, Ruoff RS (2010a) Graphene and graphene oxide: synthesis, preparation, and applications. Adv Mater 22:3906–3924

Zhu JW, Zeng GY, Nie FD, Xu XM, Chen S, Han QF, Wang X (2010b) Decorating graphene oxide with CuO nanoparticles in a water-isopropanol system. Nanoscale 2:988–994

Zu YQ, Zhao YQ, Xu KZ, Tong Y, Zhao FQ (2016) Preparation and comparison of catalytic performance for nano MgFe2O4, GO-loaded MgFe2O4 and GO-coated MgFe2O4 nanocomposites. Ceram Int 42:18844–18850